Explosive Nucleosynthesis and the Astrophysical r-Process

F.-K. Thielemann[1], C. Freiburghaus[1], T. Rauscher[1], E. Kolbe[1], B. Pfeiffer[2] K.-L. Kratz[2], and J.J. Cowan[3]

[1] *Departement für Physik und Astronomie, Univ. Basel, Klingelbergstr. 82, CH-4056 Basel, Switzerland*

[2] *Institut für Kernchemie, Univ. Mainz, Fritz-Strassmann-Weg 2, D-55099 Mainz, Germany*

[3] *Department of Physics and Astronomy, Univ. of Oklahoma, Norman, OK 73019, USA*

Abstract. We give an overview of chemical equilibria in explosive burning and the role which neutron and/or proton separation energies play. We focus then on the rapid neutron-capture process (r-process) which encounters unstable nuclei far from beta-stability with neutron separation energies in the range 1-4 MeV. Its observable features, like the abundances, witness nuclear structure as well as the conditions in the appropriate astrophysical environment. With the remaining lack of a full understanding of its astrophysical origin, parametrized calculations are still necessary. The classical approach is based on (constant) neutron number densities n_n and temperatures T over duration timescales τ. Recent investigations, motivated by the neutrino wind scenario from hot neutron stars after a supernova explosion, followed the expansion of matter with initial entropies S and electron fractions Y_e over expansion timescales τ. We compare the similarities and differences between the two approaches with respect to resulting abundance features and their relation to solar r-process abundances. Special emphasis is given to the questions (i) whether the same nuclear properties far from stability lead to similar abundance patterns and deficiencies in both approaches and (ii) whether some features can also provide clear constraints on the permitted astrophysical conditions.

INTRODUCTION

Hydrostatic burning stages in stellar evolution, like H, He, C, and Ne-burning with temperatures being essentially confined to $T<10^9$ K, are dominated by individual nuclear reactions and the precision of their cross sections.

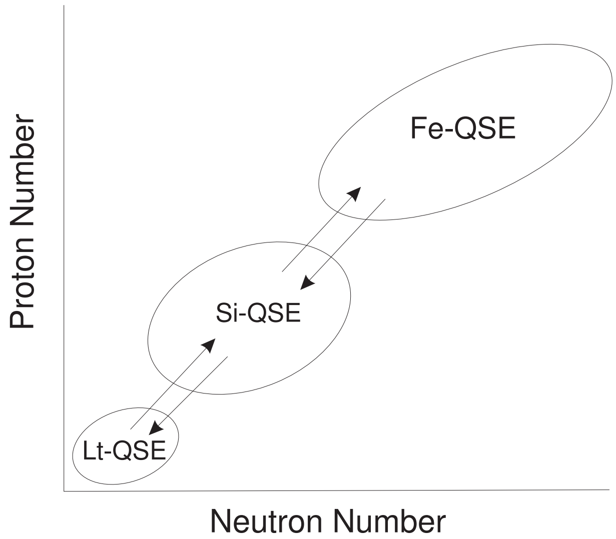

FIGURE 1. A schematic view of the nuclear chart with three quasi-equilibrium groups, (i) light nuclei including neutrons, protons and alpha partciles, (ii) the Si-group extending from Mg to the N=20 and Z=20 boundaries, (iii) the Fe-group containing nuclei above these boundaries.

The same is true for explosive events which never surpass critical temperatures. This is the case e.g. for explosive H-burning in novae which is limited to temperatures $T < 3\times10^8$ K or explosive burning stages up to Ne-burning in supernovae. Other explosive events attain high temperatures, but during their ignition stages individual reactions matter strongly. This is the case e.g. during the ignition stages of explosive H-burning in X-ray bursts, where break-out reactions from the hot CNO-cycle (bridging the gap between CNO nuclei and Ne) as well as other hot CNO-type cycles up to Ca or Ti are important. It also applies to central C-ignition in white dwarf progenitors of type Ia supernovae.

However, a whole variety of burning processes responsible for the abundances of intermediate and heavy nuclei, like e.g. hydrostatic Si and explosive O and Si-burning, are leading to partial or full equilibria of reactions. The abundances within an equilibrated reaction chain can be described by the chemical potentials of nuclei ($A + B \leftrightarrow C + D$ leads to $\mu_A + \mu_B = \mu_C + \mu_D$) which form a Boltzmann gas, being dependent on density, temperature, mass, and abundance of a nucleus. The abundance ratios are (besides thermodynamic environment properties) determined by mass differences, i.e. Q-values of reactions. Therefore, mass uncertainties matter, but uncertainties in cross sections do not enter abundance determinations [2,49]. Fig. 1 shows a schematic view of the nuclear chart with three such quasi-equilibrium (QSE) groups, as they occur in hydrostatic Si or explosive O and Si-burning. These groups are in equilibrium for neutron and proton captures. This implies equilibria also for other target nuclei as well as for mixed reactions like (p, α) etc. The reason for the equilibrium regions are fast forward and reverse reaction rates for such environment conditions, the non-equilbrium regions are identified by small cross sections and reaction rates. This is due to small Q-values for reactions out of the magic numbers N=20 and Z=20 and due to small level or resonance densities for light nuclei up to Ne. For sufficiently high temperatures, the Si and Fe-groups, or even all groups, can merge to a full or nuclear statistical equilibrium (NSE).

The chemical equilibrium for neutron or proton captures leads to abundance maxima at specific neutron or proton separation energies

$$\frac{Y(A+1)}{Y(A)} \approx 1 = n_{n,p} \frac{G(A+1)}{2G(A)} \Big[\frac{A+1}{A}\Big]^{3/2} \Big[\frac{2\pi\hbar^2}{m_u kT}\Big]^{3/2} \exp(S_{n,p}(A+1)/kT) \quad (1)$$

$$\frac{S_{n,p}(A+1)}{kT} = 24 \ln\Big[(\frac{A}{A+1})^{3/2}(\frac{G(A)}{G(A+1)})^{3/2}(\frac{T}{10^9\mathrm{K}})^{3/2}\frac{N_A}{n_{n,p}/\mathrm{cm}^3}\Big]. \quad (2)$$

The equations are valid for neutron and/or proton captures, as indicated by the n,p subsripts. The Y's are abundances related to number densities n via $n = \rho N_A Y$. At the maximum in an isotopic or isotonic line we have $S_{n,p} \approx 24kT$, if the partition functions G are neglected (order unity). This is slightly modified by logarithmic dependences on density and temperature, i.e. for higher densities the equilibrium is pushed to smaller separation energies (closer to drip lines in extreme cases). When an equilibrium with neutrons and protons exists, the abundance maximum is found in the nuclear chart at the intersection of the relevant neutron and proton separation energies. The free neutron and proton densities reflect the total neutron/proton ratio in matter, which is determined by slow, weak interactions not in equilibrium. Thus, weak interactions affect abundances by changing Y_e, the total proton/nucleon ratio $Y_e = <Z/A> = \sum Z_i Y_i / \sum A_i Y_i = \sum Z_i Y_i$. $\sum A_i Y_i$ is the sum of all mass fractions (abundance $\times$ mass number) and thus equal to 1.

The understanding that explosive burning stages are governed by QSE or even NSE is growing [52,16,17,50]. This has been shown recently in calculations of type II supernova nucleosynthesis [55,20] with two libraries of nuclear reaction rates [53,47], differing by up to factors of 5-7. Of the nuclei produced in explosive O and Si-burning, i.e. most nuclei from Si to beyond Fe, only abundance differences were noticed in the transition region between the Si and Fe groups. Different types of QSE-groups can emerge in explosive burning. The high temperature phase of the rp-process in X-ray bursts witnesses isotonic lines in $(p,\gamma)-(\gamma,p)$ equilibrium, because neutrons are not available in hydrogen-rich layers [43,41] (see also Wiescher, this volume). The (slow) weak interactions are not in equlibrium and thus the β^+-decays (and also some connecting and competing (α,p) reactions) have to be followed explicitely. Another application is the r-process which should be the focus of the rest of this contribution. Here the QSE-groups are isotopic lines in $(n,\gamma)-(\gamma,n)$ equilibrium, and the connecting weak interactions are β^--decays. It should be mentioned that during the final stages when freeze-out from equilibria occurs due to the expansion of matter and temperature decline below equilibrium conditions, reaction rates count again. But the abundance differences will be smaller than expected from rate differences.

In general it should be pointed out that equilibria simplify the understanding of explosive nucleosynthesis processes and individual cross sections play a much less important role than reaction Q-values, i.e. mass differences. However, opposite to environments with neutron/proton ratios favoring nuclei close to stability, processes like the rp and r-process explore exotic nuclei close to the neutron or proton drip-lines where masses are not well known. Therefore the focus lies on nuclear masses and beta-decay properties and their experimental and theoretical investigations (see also Kratz and Wiescher, this volume).

R-PROCESS BASICS

The question whether we understand fully all astrophysical sites leading to an r-process is not a settled one. It is usually assigned type II supernovae (SNe II), the events accompanying the deaths of massive stars and formation of neutron stars (high entropy ejecta, see [56,46]). But galactic evolution timescales and the delayed emergence of r-process matter indicate that these can probably only be SNe II with long evolution timescales at the lower limit of supernova progenitor masses ($\sim$8-10 $M_\odot$) [7,28], while neutron star mergers or still other low entropy sites are not necessarily excluded [27,29,9]. Both these environments provide or can possibly provide high neutron densities and high temperatures which ensure an $(n,\gamma)-(\gamma,n)$ equilibrium in each isotopic chain before the decline of densities and temperatures during the explosion. However, recent observations shed some doubts on the supernova origin. On average type II supernovae produce Fe to intermediate mass elements in ratios within a factor of 3 of solar [49]. If they would also be responsible for the r-process, the same limits should apply. But the observed bulk r-process/Fe ratios vary widely in low metallicity stars. For example CS 22892–052 has an r/Fe ratio which is 30 times larger than solar [44]!

For the r-process source discussion ist is also helpful to ask the question which abundance pattern we need to explain. There are (i) the present r-process abundances in the solar system and (ii) elemental abundance observations of low metallicity stars. The latter are very old stars and display with their unchanged surface abundances the composition of the interstellar medium early in galactic evolution. The observations of low metallicity stars are all consistent with the solar r-abundance pattern of elements and the relative abundances among heavy elements do apparently not show any time evolution [44,6], at least for elements heavier than Ba. The analysis of Ba line profiles in several metal-poor stars showed that also the ratio of odd to even isoptopes agrees with a solar r-process distribution (making use of hyperfine splitting for odd isotopes [10]). This, plus the reproduction of the third

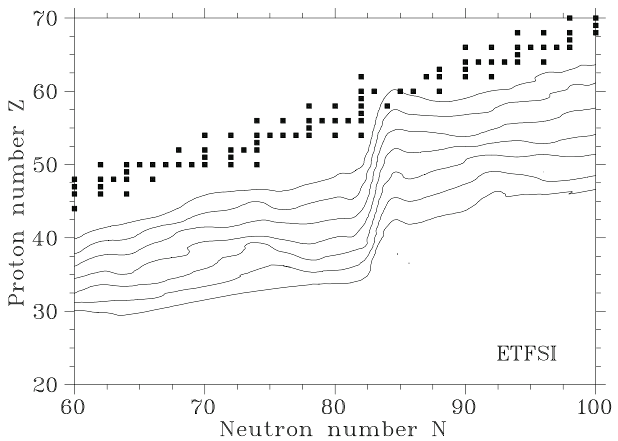

FIGURE 2. Contour plots of constant neutron separation energies S_n=1,2,3,4,5,6, and 7 MeV in the $80 \leq A \leq 140$ mass region for the ETFSI mass model [1]. Note the saddle point behavior caused by the shell closure at $N = 82$, also existing when using the FRDM masses [34], which leads to a deep trough before the peak at $A = 130$ (see dashed line in Fig. 3).

r-process peak (Os, Ir, Pt) suggests strongly that (at least beyond Ba) all contributing astrophysical events have a solar r-process composition, opposite to different claims [14]. Even if all events contributing to galactic evolution produce the same relative r-process abundances, a single astrophysical site will still have varying conditions in different ejected mass zones. This naturally guides towards a multi-event model (where all events are close to identical), however, each event displays a multi-component (i.e. superposition) behavior. A component is defined by a combination of neutron number density, temperature (defining the neutron separation energy of an r-process path) and duration time, or more physically for an adiabatic expansion, entropy, Y_e, and an expansion timescale. The physical conditions must vary smoothly, as expected from a single astrophysical site, opposote to other assumptions [13].

The site-independent classical analysis of Kratz et al. [23,24], based on n_n, T, and τ, led to the conclusion that the r-process experienced a fast drop from equilibrium (of the order of 0.05 s, at least for conditions producing the $A \simeq 80$ peak), in order not to wash out the odd-even staggering via slow freeze-out effects. A continuous superposition of components with neutron separation energies in the range 4-2 MeV (see Eq.(2), related to n_n and T) on timescales of 1 - 2.5 s, provided a good overall fit. The beta-decay properties along contour lines of constant S_n towards heavy nuclei [48] (see Fig. 2 for the region around the N=82 shell closure) are responsible for the resulting abundance pattern. These are predominantly nuclei not accessible in laboratory experiments to date. Exceptions exist in the A = 80 and 130 peaks [23,24] and continuous efforts are underway to extend experimental information in these regions of the closed shells N=50 and 82 with radioactive ion beam facilities (e.g. Kratz, this volume). Such classical r-process studies were extended to deduce necessary

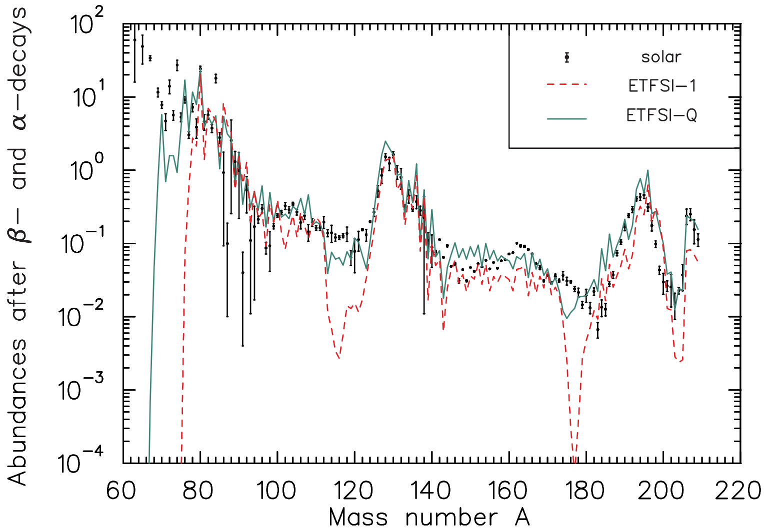

FIGURE 3. Fits to solar r-process abundances [22], obtained with a smooth superposition of 17 equidistant $S_n(n_n,T)$ components from 1 to 4 MeV. The dashed line presents the results for ETFSI masses [1] with half-lives $\tau_{1/2}$ and beta-delayed neutron emission P_n values from QRPA calculations [33]. For the solid line the ETFSI-Q mass model [36] was applied, which introduced a phenomenological quenching of shell effects. The quenching of the $N=82$ shell gap leads to a filling of the abundance troughs. These results [37] are also the first ones which show a good fit to the r-process Pb and Bi contributions after following the decay chains of unstable heavier nuclei.

requirements for nuclear properties like masses, half-lives, and deformation [48,5,37,25]. One of the major conclusions was the quest for shell quenching far from stability in order to avoid abundance deficiencies, as seen in Fig. 3.

ENTROPY BASED CALCULATIONS

For the operation of an r-process 10 to 150 neutrons per seed nucleus (in the Fe-peak or somewhat beyond) have to be available to form all heavier r-process nuclei by neutron capture. For a composition of Fe-group nuclei and free neutrons that translates into a $Y_e = <Z/A> = 0.12$-0.3. Such a high neutron excess is not existing in typical stellar environments and only possible for high densities in neutron stars under beta equilibrium ($e^- + p \leftrightarrow n + \nu$) with neutrino escape and $\mu_e + \mu_p = \mu_n$, based on the high electron Fermi energies (chemical potentials) which are comparable to the neutron-proton mass difference [4,29].

Another option is a so-called extremely alpha-rich freeze-out in complete Si-burning with moderate Y_e>0.40. After the freeze-out of charged particle reactions in matter which expands from high temperatures but relatively low densities, e.g. 90% of all matter can be locked into ^{4}He with N=Z, which leaves even for moderate Y_e's a large neutron/seed ratio for the few existing heavier nuclei. This corresponds to a freeze-out from QSE in Fig. 1 where

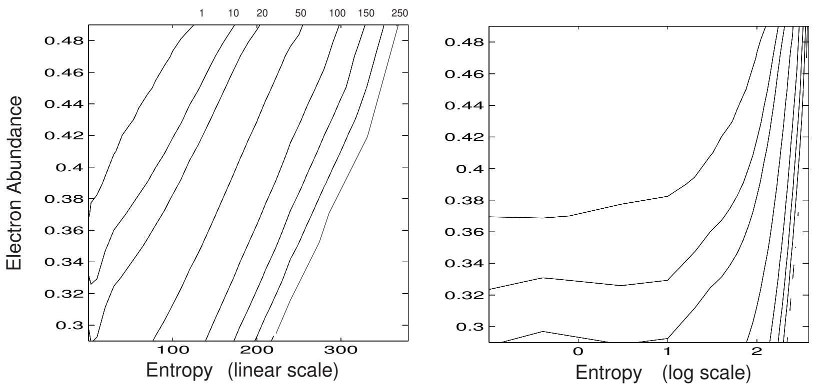

FIGURE 4. Y_n/Y_{seed} contour plots as a function of intial entropy S and Y_e for an expansion time scale of 0.05s. The left part shows how, for moderate Y_e-values, an increasing neutron/seed ratio, indicated by contour lines labeled with the respective Y_n/Y_{seed}, can be attained with increasing entropy which leads to a stronger alpha-rich freeze-out behavior. The results scale with Y_e, measuring the global neutron/nucleon ratio 1-Y_e. The right part of the figure enhances on a logarithmic scale the low entropy behavior, where Y_n/Y_{seed} is only determined by the electron abundance Y_e. The contour lines are the same for both figures. A Y_n/Y_{seed} ratio of 150, which produces the heaviest r-process nuclei, would only be attained for a Y_e as small as 0.12.

groups 2 and 3 merged, but the connection between 1 and 2 is extremely weak due to low densities. The links accross the particle-unstable A=5 and 8 gaps is only possible via the three body reactions $\alpha\alpha\alpha$ and $\alpha\alpha n$ to ^{12}C and ^{9}Be, whose reaction rates show a quadratic density dependence. The entropy per gram of baryons in a radiation dominated gas is proportional to T^3/ρ and can be used as a measure of the ratio between the remaining He mass-fraction and heavy nuclei. $S{\sim}0.15$ k_B/nucleon represents the deviding line between a normal and alpha-rich freeze-out. Similarly, the ratio of neutrons to heavy nuclei (i.e. the neutron to seed ratio) is a function of entropy and permits for high entropies, with large remaining He and neutron abundances compared to small heavy seed abundances, neutron captures which proceed to form the heaviest r-process nuclei [54,32,46,56,18,19].

The behavior of these latter two environments, representing a normal and alpha-rich freeze-out, is summarized in Fig. 4. The available number of neutrons per heavy nucleus Y_n/Y_{seed} after charged particle freeze-out, when the lerge QSE-groups break up into isotopic lines, is shown as a function of entropy and initial Y_e. At low entropies the transition to a normal freeze-out occurs, indicated by the negligible entropy dependence. Recent r-process studies [56,46,38,19] have concentrated on the high entropy environment in the innermost ejecta of SNe II. These are the layers heated by neutrino emission and evaporating from the hot proto-neutron star after core collapse. Whether the entropies required for these conditions can really be attained in supernova explosions has still to be verified. In order to investigate the questions, whether

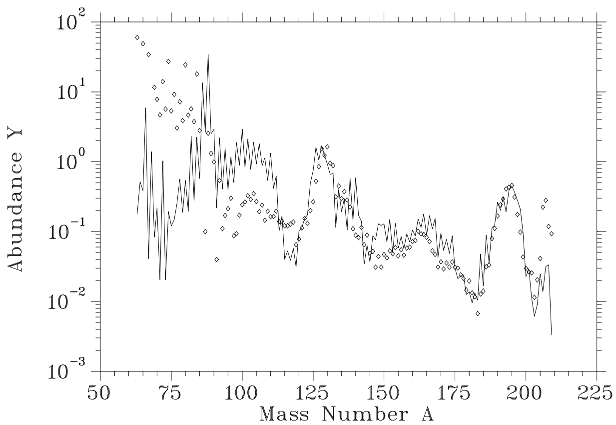

FIGURE 5. Similar to Fig. 3 with the ETFSI mass formula, making use of a superposition of entropies $g(S)$ to attain an overall good fit to solar r-process abundances from a high entropy neutrino wind in type II supernovae. These calculations were performed with $Y_e = 0.45$, but similar results are obtained in the range $0.30 - 0.49$, only requiring a scaling of entropy. The trough below $A = 130$ behaves similar to Fig. 3. This shows that a time dependent freeze-out (with a full treatment of neutron captures and photodisintegrations), resulting from a scenario based on entropy, can cause the same abundance deficiencies due to specific nuclear structure features as obtained in the site-independent classical approach with an instantaneous freeze-out from $(n, \gamma) - (\gamma, n)$-equilibrium.

and how explosion entropies can be translated into n_n and T (or S_n) of the site-independent classical approach, we performed a parameter study based on the entropy S and Y_e, in combination with an expansion timescale of typically 0.05 s [46], and varied nuclear properties (i.e. mass models). The neutron capture rates were calculated with the statistical model code SMOKER [40]. The β^--rates came from experimental data or QRPA calculations [33].

Following the reasons discussed above, we chose a smooth superposition with a weighting function $g(S_i) = x_1 e^{-x_2 S_i}$, where the index i counts the components. Fig. 5 shows a Y_e=0.45 sequence. Entropies from about 200 to about 350 give Y_n/Y_{seed}-ratios growing from approximately 30 to 150. The α-rich freeze-out always produces seed nuclei in the range $90 < A < 120$. This material can then be "r-processed", leading to a fully neutron dominated process, and the components have a very similar abundance pattern in the mass range A=110 - 200, as found in the classical approach. Thus, it is possible for this entropy range to establish a one-to-one correspondence for abundances obtained via entropy and expansion timescale (S, τ) in one type of calculation and neutron separation energy and timescale $(S_n(n_n, T), \tau)$ in classical calculations. The neutron separation energy S_n of the r-path is the one obtained during neutron capture freeze-out in the entropy based calculations.

Different mass models (in Fig. 5 only ETFSI [1] is shown) give fits of similar quality as in the site-independent classical approach. The discrepancies below the $A = 130$ r-process peak, in form of a pronounced trough, occur again for

FRDM [34] and ETFSI. Thus, our earlier conclusions can be translated from the classical analysis to realistic astrophysical applications in this mass region. The nuclear structure properties leading to agreement and deficiencies apply in the same way, due to the nature of a fast freeze-out, which preserves the abundances as they result from an initial (n,γ)-(γ,n)-equilibrium at high temperatures, even when neutron captures and photodisintegrations are followed individually [11]. There is possibly one difference to the conclusions given with Fig. 3. The calculations experiencing the highest entropies have the longest neutron freeze-out timescales and are responsible for the heaviest nuclei [11]. Our results show that the trough before the $A=195$ peak, resulting in case of the ETFSI mass model and the classical approach, does not survive [48,5,3,37]. This region is changed by ongoing (non-equilibrium) neutron captures during the freeze-out and apparently does not directly witness nuclear properties far from stability at the $N=126$ shell closure (Fig. 5). This outcome might change, however, back to the classical approach, as giant dipole resonance features based on neutron skins of neutron-rich nuclei far from stability could enhance neutron capture cross sections tremendously and ensure the existence of an $(n,\gamma)-(\gamma,n)$ equilibrium to lower temperatures [12].

There have been suggestions that neutrino-induced spallation of nuclei in the $A=130$ peak, caused by a strong neutrino wind from the hot neutron star, could fill abundance troughs [39]. We refer to a more detailed discussion of this effect [11], including the requirements on neutrino luminosities and distances of ejecta from the neutron star at the time of the neutron freeze-out. We come to the conclusion in agreement with [39] that this effect can only be of importance for the low mass wings of the A$\sim$130 peak, but not for the mass region in the range 110-120. Nuclear structure effects (shell quenching far from stability) seem to be the best solution, especially as they are already observed experimentally and predicted theoretically [35,45,57,21,8,26]. For a general review whether neutrino interactions with matter actually support or hinder the occurance of an r-process see [31].

The correspondence between classical and entropy based calculations can only be established for entropies producing nuclei with $A>$110. Matter with $A<$110 results from lower entropies with a neutron-poor and alpha-rich freeze-out, where the abundances of heavy nuclei are dominated by those with alpha separation energies of $\approx$6 MeV [11]. This follows from an equation very similar to Eq.(2) for alpha separation energies. None of these entropies produces an abundance peak at charged particle freeze-out with $A<80$, leaving a sufficient amount of neutrons for r-processing which would reproduce the typical neutron-induced abundance features in the range $A=80-110$. A different choice of Y_e (e.g. 0.49) can influence that pattern somewhat in avoiding very large spikes for $A\approx90$ and N=50 isotopes, but the overall features stay. Within an entropy based approach only conditions with lower Y_e, but also lower entropies, can lead to abundance features in agreement with the solar r-abundance pattern similar to the classical approach. Such features relate to

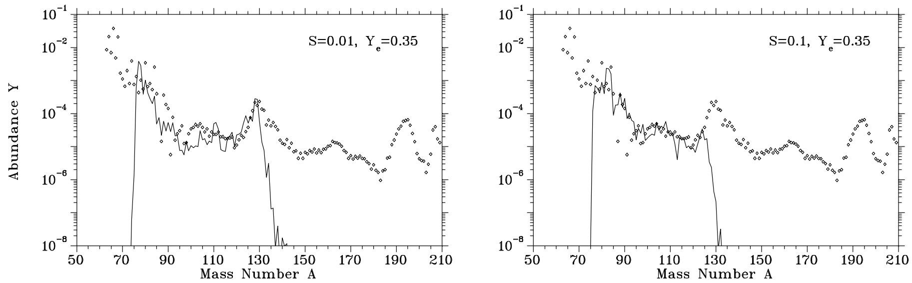

FIGURE 6. A low $Y_e = 0.35$ value and a high density $\rho > 10^7\,\mathrm{g\,cm^{-3}}$ cause a normal (low-entropy) freeze-out with a sufficient amount of neutrons left for the synthesis of $80 < A < 120$ nuclei. This calculation utilized a droplet model [15] which similar to ETFSI-Q avoids the trough for $110 < A < 120$. A further decrease in Y_e (see Fig. 4b) will increase the Y_n/Y_{seed}-ratio and could also account for the upper mass range of r-process nuclei. Such an environment is similar to low entropy scenarios related to neutron stars [7,30,42].

nuclei along contour lines of constant neutron (rather than alpha) separation energies (Fig. 6).

CONCLUSIONS

The r-process is a typical example of an explosive burning environment determined by reaction equilibria and particle separation energies. Its abundance features reflect the beta-decay half-lives along contour lines of constant neutron separation energy, which led to the classical site-independent approach based on a constant neutron number density n_n and temperature T over a process duration time τ. More realistic astrophysical environments are expected to follow the expansion of matter with initial entropies S on expansion timescales τ through the freeze-out of reactions with declining temperatures and densities. While this has been performed before by a number of investigators, it is the first time that different mass models have been explored in such investigations.

We find essentially a one-to-one mapping between the results of the classical and the entropy based approach for entropies producing nuclei with mass numbers $A>110$. The neutron separation energy of the r-path at neutron freeze-out is the same as in the corresponding classical components with constant n_n and T. Concerning the influence of nuclear properties far from stability, the conclusions of the classical site-independent calculations of [24,5,37] remain valid for the $A \simeq 130$ region and the abundance troughs can be cured by quenching of shell effects.

However, for high entropy environments, as expected from a high entropy neutrino wind in supernovae, there exists no correspondence for contributions which cover the mass range $80 < A < 110$. They are the product of charged particle reactions and a neutron-poor, alpha-rich freeze-out. It is not meaningful to compare these contributions to classical r-process calculations and the resulting abundances do not fit the solar r-abundance pattern either. Low entropies $S < 0.1$ and low Y_e's of the order of ≤ 0.35, which lead to a normal (i.e. not alpha-rich) freeze-out, can provide neutron densities that resemble classical r-process studies and produce a good fit to the solar abundance pattern in the mass range of $80 < A < 120$. The latter findings seem to exclude high entropy supernova environments for producing the mass region $80 < A < 110 - 120$. This could point towards low entropy sources related to expanding neutron star matter.

Whether such an interpretation ($A < 130$ from low Y_e and S conditions, $A > 130$ from high S conditions) is a solution, might eventually be answered by observations. There seems to exist meteoritic evidence from the extinct radioactivities ^{107}Pd, ^{129}I, and ^{182}Hf [51] that the last r-process contributions to the solar system for $A > 130$ and $A < 130$ came at different times, i.e. from different types of events. It is highly desirable to have an independent verification from observations of low metallicity stars, which apparently show a completely solar r-process composition for nuclei with $A > 130$ [44,6].

ACKNOWLEDGMENT

This work was supported by the Swiss Nationalfonds (grant 20-47252.96 and 2000-053798.98), the German BMBF (grant 06Mz864) and DFG (grant Kr80615), the US NSF (grant AST 9618332) and the Austrian Academy of Sciencies.

REFERENCES

1. Aboussir, Y. et al. 1995, At. Data Nucl. Data Tables, 61, 127
2. Arnett, W.D. 1996, *Nucleosynthesis and Supernovae*, Princeton Univ. Press
3. Bouquelle, V. et al. 1996, A & A, 305, 1005
4. Cameron, A.G.W. 1989, AIP Conf. Proc. 183, 349
5. Chen, B. et al. 1995, Phys. Lett., B355, 37
6. Cowan, J.J., McWilliam, A., Sneden, C., Burris, D.L. 1997, Ap. J., 480, 246
7. Cowan, J. J., Thielemann, F.-K., Truran, J. W. 1991, Phy. Rep., 208, 267
8. Dobaczewski, J. et al. 1996, Phys. Rev. C53, 2809
9. Eichler, D., Livio, M., Piran, T., Schramm, D. N. 1989, Nature, 340, 126
10. Francois, P. & Gacquer, W. 1998, Nature, in press
11. Freiburghaus, C. et al. 1998, Ap. J., in press
12. Goriely, S. 1998, Phys. Lett. B, in press
13. Goriely, S., Arnould, M. 1996, A & A, 312, 327
14. Goriely, S., Arnould, M. 1997, A & A, 322, L29
15. Hilf, E. R., von Groote, H., & Takahashi, K. 1976, CERN-Rep 76-13, p.142
16. Hix, W.R., Thielemann F.-K. 1996, Ap. J. 460, 869
17. Hix, W.R., Thielemann F.-K. 1998, Ap. J., in press

18. Hoffman, R. D. et al. 1996, Ap. J., 460, 478
19. Hoffman, R. D., Woosley, S. E., Qian, Y.-Z. 1997, Ap. J., 482, 951
20. Hoffman, R. D., Woosley, Weaver, T.A., Rauscher, T. Thielemann, F.-K. 1998, Ap. J., submitted
21. Ibbotson, R.W. et al. 1998, Phys. Rev. Lett. 80, 2081
22. Käppeler, F., Beer, H., Wisshak, K. 1989, Rep. Prog. Phys. 52, 945
23. Kratz, K.-L. et al. 1988, J. Phys. G, 14, 331
24. Kratz, K.-L. et al. 1993, Ap. J. 402, 216
25. Kratz, K.-L., Pfeiffer, B., Thielemann, F.-K., 1998, Nucl. Phys. A630, 352c
26. Lalazissis, G.A., Vretenar, D., Ring, P. 1998, Phys. Rev. C57, 2294
27. Lattimer, J. M. et al. 1977, Ap. J., 213, 225
28. Mathews, G.J., Bazan, G., Cowan, J.J. 1992, Ap. J. 391, 719
29. Meyer, B. S. 1989, Ap. J., 343, 254
30. Meyer, B. S. 1994, Ann. Rev. Astron. Astrophys, 32, 153
31. Meyer, B.S., McLaughlin G.C., Fuller, G.M. 1998, Phys. Rev. C, in press
32. Meyer, B.S. et al. 1992, Ap. J 399, 656
33. Möller, P., Nix, J.R., Kratz, K.-L. 1997, At. Data Nucl. Data Tables 66, 131
34. Möller, P. et al. 1995, At. Data Nucl. Data Tables 59, 185
35. Orr, N. A. 1991, Phys. Lett. B258, 29
36. Pearson, J. M., Nayak, R. C., Goriely, S. 1996, Phys. Lett. B387, 455
37. Pfeiffer, B., Kratz, K.-L., Thielemann, F.-K. 1997, Z. Phys. A357, 235
38. Qian, Y.-Z., Woosley, S. E. 1996, Ap. J., 471, 331
39. Qian, Y.-Z., Haxton, W.C., Langanke, K., Vogel, P. 1996, Phys. Rev. C55, 1532
40. Rauscher, T., Thielemann, F.-K., Kratz, K.-L. 1997, Phys. Rev. C56, 1613
41. Rembges, F. et al. 1997, Ap. J. 484, 412
42. Rosswog, S. et al. 1998, A & A, in press
43. Schatz, H. et al. 1998, Phys. Rep. 294, 167
44. Sneden, C. et al. 1996, Ap. J. 467, 819
45. Sorlin, O. et al. 1993, Phys. Rev. C47, 2941
46. Takahashi, K., Witti, J., Janka, H.-T. 1994, A&A, 286, 857
47. Thielemann, F.-K., Arnould, M., Truran, J. W. 1987, in *Advances in Nuclear Astrophysics*, ed. E. Vangioni-Flam, Gif sur Yvette, Editions Frontière, p.525
48. Thielemann, F.-K. et al. 1994, Nucl. Phys. A570, 329c
49. Thielemann, F.-K. et al. 1998, in *Nuclear and Particle Astrophysics*, eds. J. Hirsch, D. Page, Cambridge Univ. Press, p.27
50. Wallerstein, G. et al. 1997, Rev. Mod. Phys. 69, 995
51. Wasserburg, G., Busso, M., Gallino, R. 1996, Ap. J. 466, L109
52. Woosley, S.E., Arnett, W.D., Clayton, D.D. 1973, Ap. J. Suppl. 26, 231
53. Woosley, S.E. et al. 1978, At. Data Nucl. Data Tables 22, 371
54. Woosley, S. E., Hoffman, R. D. 1992, Ap. J. 395, 202
55. Woosley, S.E. et al. 1997, Nucl. Phys. A621, 445c
56. Woosley, S. E. et al. 1994, Ap. J. 433, 229
57. Zhang, C.T. et al. 1997, Z. Phys. A358, 9